Natural Hazards and Earth System Sciences (2003) 3: 341–351

Natural Hazards and Earth System Sciences

Sensitivity of the adjoint method in the inversion of tsunami source parameters

C. Pires and P. M. A. Miranda

Department of Physics and Centro de Geofisica, University of Lisbon, Campo Grande, 1749-016, Lisbon, Portugal

Received: 8 October 2002 – Accepted: 19 November 2002

Abstract. This paper tests a methodology for tsunami waveform inversion, based on the adjoint method. The method is designed to perform the direct optimization of the tsunami fault parameters, from tide-gauge data, imposing strong geophysical constrains to the inverted solutions, leading to a substantial enhancement of the signal-to-noise ratio, when compared with the classical technique based on Green's functions of the linear long-wave model. A 4-step inversion procedure, which can be fully automated, consists (i) in the source area delimitation by adjoint backward ray-tracing, (ii) adjoint optimization of the initial sea state, from a vanishing first-guess, (iii) non-linear adjustment of the fault model and (iv) final adjoint optimization in the fault parameter space. That methodology is systematically tested with four different idealized bathymetry and coastline setups (flat bathymetry in an open domain, closed conical circular lake, islands in an open domain and submarine mountains in an open domain) and different amounts of synthetic observation data, and of observational and bathymetric errors. Results show that the method works well in the presence of reasonable amounts of error and it provides, as a by-product, a resolution matrix that contains information on the inversion error, identifying the combinations of source parameters that are best and worst resolved by the inversion.

1 Introduction

Tide gauge data provides information on the location and geometry of tsunami sources that can be used to improve our understanding of the geophysical processes, which are at the origin of the tsunami generation. Different methods for tsunami inversion have been proposed in the past. Abe (1973) developed a backward ray-tracing technique, only requiring the knowledge of the tsunami arrival times, which has been successfully used to locate the boundaries of the source. Backward ray-tracing is unable to give any information on the source shape. Satake (1987, 1989) used Green's functions technique to invert the coseismic slip, in a set of simple prescribed rectangular sub-faults, from observed tide gauge data. Jonhson et al. (1996) and Johnson (1999) extended that technique to the joint adjustment of tide gauge and geodetic data. Very recently, Piatanesi et al. (2001), following an earlier work by Tinti et al. (1996), performed an extensive set of sensitivity experiments with synthetic data, using finite elements as distributed point sources. Koike and Imamura (2001) proposed a wavelet basis for the sub fault distribution, which allows for a better adjustment of consistent geophysical sources with a smaller number of independent parameters. All these methods assumed that the initial water elevation field is a linear combination of a set of basis function and also that the propagation model is linear.

Pires and Miranda (2001), hereafter referred as PM01, proposed a more general approach to the tsunami inversion problem, making use of the adjoint technique, which has been gaining increasing importance for atmospheric and oceanic data assimilation (cf. the thorough reviews by Ghil and Malanotte-Rizzoli, 1991; Bennet, 1992; Wunsch, 1996) and in non-linear inverse problems (Pires et al., 1996). The adjoint method can be used with non-linear propagation models and it can invert initial fields that are non-linear functions of the independent parameters. On the other hand, the method does not require a good first guess for the fault distribution, necessary in Satake's (1987) approach, and the computational cost is not overwhelmed by the need to compute a large number of Green's functions corresponding to every grid point in the domain.

As shown by PM01, the adjoint method can be used for the inversion of distributed sources, in a context quite similar to the one shown by Piatanesi et al. (2001). In the case of distributed sources it is always necessary to constrain the source location in order to obtain a well-conditioned problem, as shown later in this paper. In general, those constraints have been obtained by the addition of independent geophysical data. However, a set of single integrations of the adjoint model provides an objective way to locate the source bound-

Correspondence to: P. Miranda (pmiranda@fc.ul.pt)

aries, by "adjoint ray-tracing", later explained.

Another, and most relevant characteristic of the adjoint method, is the possibility of direct optimization of the fault parameters, allowing for a strong reduction of the inversion error and for the elimination of spurious sources. Seismic tsunamis give important information about great submarine earthquakes, complementing geophysical data. For those tsunamis, the initial sea-bed deformation in a homogeneous media can be approximated by an analytical model proposed by Okada (1992), which is a non-linear function of 9 fault parameters, describing the fault location, extension and shape. The adjoint method can also be used to directly optimize those parameters.

This paper tests the methodology proposed by PM01 in a series of systematic numerical experiments with synthetic data, where some advantages of the method are explored in some detail and its sensitivity to bathymetric fields, observational and bathymetric errors, source geometry, number of tide gauges, assimilation frequency and extent of the assimilation interval, are assessed. At the same time, those experiments address some known problems in waveform inversion, proposing and testing methodologies to deal with them in the context of the adjoint technique.

Historical tsunamis may provide useful information for seismic risk assessment, because they are linked to great submarine earthquakes, which, although infrequent, contribute very much to the total risk. In some cases (e.g. Baptista et al., 1998), especially when direct seismic observations are absent or scarce, the inversion of tsunami data may usefully constrain the seismic source parameters.

The paper is organized as follows. In Sect. 2 the adjoint method is briefly explained. Section 3 presents the setup of the numerical experiments. Section 4 presents results from a set of unconstrained inversions for different bathymetric fields, putting in evidence the intrinsic ill-conditioning of the inversion problem in an open domain, and the difficulties of the inversion in steep slopes and closed boundaries. Section 5 explains the source delimitation by the adjoint method and tests its performance in the same set of bathymetric fields. Section 6 presents results from the sensitivity experiments with constrained distributed sources. Section 7 proceeds with the inversion of fault parameters and the computation of the corresponding resolution matrix and its eigen-decomposition. The paper concludes in Sect. 8, with a discussion of the main results.

2 Inversion method

The inversion problem in tsunami modelling can be stated as follows: given a set of tide gauge series, find the best initial water displacement field that leads to propagating waveforms that optimally fits the observations at later times. The problem is similar to the 4D-var data assimilation problem in atmospheric and oceanic models (Talagrand and Courtier, 1987) that uses the integration of the linearized adjoint model to compute the gradient of the misfit between observations and simulated series.

It is possible to compute an adjoint model for any forward propagation model. In this study one will use for simplicity the linear shallow water model:

$$\begin{aligned} \partial_t \varsigma &= -\nabla \cdot (h\boldsymbol{v}) \\ \partial_t \boldsymbol{v} &= -g\nabla\varsigma \end{aligned} \tag{1}$$

with boundary conditions:

$$\boldsymbol{v}\cdot\boldsymbol{n} = 0 \text{ on a solid boundary defined by the normal } \boldsymbol{n} \tag{2a}$$

$$\frac{\partial \boldsymbol{v}}{\partial n} = 0 \text{ on an open boundary defined by the normal } \boldsymbol{n}, \tag{2b}$$

where $\boldsymbol{v} = (u,\ v)$ is the horizontal fluid velocity vector, in the x and y directions respectively, ς is the water elevation above the mean sea level, h is the basin depth, g is the acceleration of gravity. Equations (1) and (2) are integrated numerically using an upstream scheme.

The inversion problem consists in the minimization of a cost function given by the square misfit between observed and simulated tide gauges, summed over the totality of observations N_{ob}, in both space and time:

$$J_{tg} = \sum_{i=1}^{N_{\text{ob}}} \left(\varsigma_i^{\text{obs}} - \varsigma_i^{\text{sim}}\right)^2. \tag{3}$$

The simulated values, ς_i^{sim}, for all time and observation points, are dependent on the initial water surface deformation field ς^{init}. All simulations assume an initial state at rest ($\boldsymbol{v} = 0$). Therefore, J_{tg} is an explicit function of the initial field, ς^{init}, with dimension equal to the number of grid points of the computational domain. However, in the general case, the full inversion is very badly conditioned, even with noise-free observations, if a reduced number of tide gauges is considered in J_{tg} (Tinti et al., 1996; Piatanesi et al., 2001).

A better inversion conditioning is obtained either by a reduction of the target area for inversion or by expressing the initial field ς^{init} in terms of a reduced number of parameters, such as: coseismic moments in a set of prescribed sub faults (Satake, 1987, 1989), the seismic parameters of the analytical Okada (1992) formulas (PM01), the initial field components over a wavelet basis (Koike and Imamura, 2001).

The cost function is, therefore, expressed in terms of a control vector $\boldsymbol{V}_{\text{inv}}$ with the parameters to invert. If $\boldsymbol{V}_{\text{inv}}$ and ς^{init} are linearly related and the forward model is linear, then the Green function technique may be applied and the inverted field is the solution of a generalized least squares problem. The adjoint method allows to relax these constraints, giving the possibility of using a non linear forward model or a non linear link between the initial field and the control vector.

The minimum of J_{tg} is obtained, iteratively, through the gradient descent method using an explicit formula for the gradient of J_{tg} with respect to the control vector $\boldsymbol{V}_{\text{inv}}$. This gradient, $\partial J_{tg}/\partial \boldsymbol{V}_{\text{inv}}$, is obtained by the adjoint method, briefly explained below.

Table 1. Fault parameters of the seismic source

Parameter	Symbol	Units	Scale
dip angle	δ	°	$180°/\pi$
depth of the middle point of the fault	d	km	150 km
dip slip dislocation	U_{sl}	m	1 m
strike slip dislocation	U_{st}	m	1 m
x-component of the middle point	x_0	km	150 km
y-component of the middle point	y_0	km	150 km
strike angle (from North)	α	°	$180°/\pi$
length of fault	L	km	150 km
width of fault	W	km	150 km

Let $(\varsigma_j,\, u_j,\, v_j)^T$ be the transposed state vector at time step j, and $(\delta\varsigma_j,\, \delta u_j,\, \delta v_j)^T$ be its perturbation. The perturbation evolves in time according to the linearized model:

$$(\delta\varsigma_{j+1},\, \delta u_{j+1},\, \delta v_{j+1}) = T_j(\varsigma_j,\, u_j,\, v_j)(\delta\varsigma_j,\, \delta u_j,\, \delta v_j), \tag{4}$$

where the T_j is a matrix representing the linearized version of the propagation model, which depends on the state vector at time step j. The gradient of J_{tg} with respect to the initial field is given by a backward integration of the linear adjoint method:

$$(\delta\varsigma_N^*,\, \delta u_N^*,\, \delta v_N^*) = \left(\frac{\partial J_{tg}}{\partial\varsigma_N}, 0,\, 0\right),$$

initialization of the adjoint model (5a)

$$(\delta\varsigma_{j-1}^*,\, \delta u_{j-1}^*,\, \delta v_{j-1}^*) = T^*(\varsigma_j,\, u_j,\, v_j)(\delta\varsigma_j^*,\, \delta u_j^*,\, \delta v_j^*),\ j = N, ..., 1, \tag{5b}$$

$$\frac{\partial J_{tg}}{\partial\varsigma_0} = \delta\varsigma_0^*, \tag{5c}$$

where N is the last instant taken in the assimilation period, $()^*$ stands for an adjoint variable and model (T_j^*), using a metric based on the mechanical energy (cf. PM01). The gradient of the cost function (5c) is the final result of the integration of the adjoint model.

In general, the minimization of J_{tg} starts from a first guess, where $J_{tg} = J_{fg}$, and proceeds by reducing J_{tg} until a stopping criterion is reached. In each iteration, a new guess for the initial state (ς_0) can be obtained by an optimization technique (such as the quasi-Newton gradient descent method, cf. Gilbert and LeMaréchal, 1989). If one decides to constrain the initial state, (5c) must be replaced by the gradient of the cost function with respect to the control vector (V_{inv}), which is obtained from (5c) by the chain rule:

$$\frac{\partial J_{tg}}{\partial V_{\text{inv}}} = \frac{\partial J_{tg}}{\partial\varsigma_0}\frac{\partial\varsigma_0}{\partial V_{\text{inv}}}, \tag{6}$$

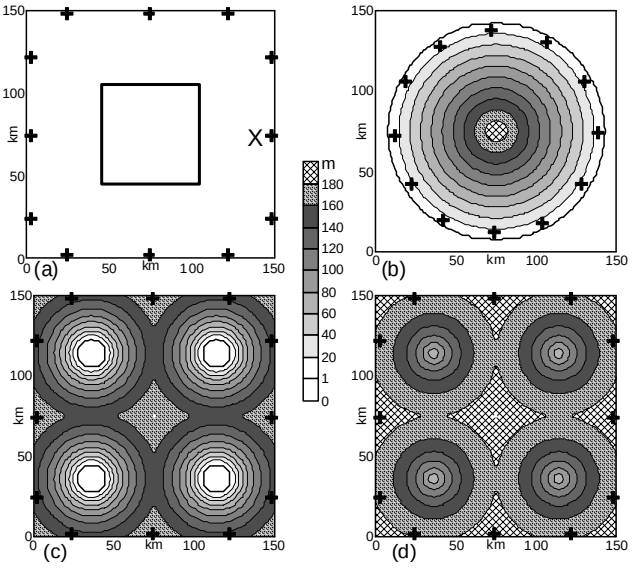

Fig. 1. Bathymetry and tide gauge location in the inversion experiments: **(a)** flat bathymetry in an open domain, square indicates the area of the constrained source; **(b)** closed lake; **(c)** islands in an open domain; **(b)** submarine mountains in an open domain.

where the summation convention was assumed, and the optimization proceeds in the V_{inv} space. In unconstrained inversions the control vector coincides with ς_0, and (6) is identical to (5c). In spatially delimited inversions V_{inv} is a subset of ς_0. In the case of seismic tsunamis, V_{inv} may be the set of Okada fault parameters for one or more faults.

When one uses a control vector whose components have different physical dimensions, which is the case of the Okada (1992) model, it is necessary to adimensionalize the control vector components. In this study, two single faults were assumed, with 9 independent parameters listed in Table 1. The scales for each parameter were chosen to ensure that similar changes in all non-dimensional parameters will lead to comparable sea-bed deformations, which is necessary to improve the conditioning of the minimization (PM01).

The inversion of real tsunamis must be able to deal with experimental errors of different origin. These include: tide gauge observation errors, bathymetric and model errors. The presence of errors implies that the cost function will not converge to zero and so one must define a stopping criterion for the iteration taking into account the existence of a significant noise level. Let σ_{ob}^2 be the variance of the observation error at the tide gauges. The iterations will be stopped when either of the following conditions is reached:

$$\frac{J_{tg}}{N_{ob}\sigma_{ob}^2} < P_{95}\sqrt{\frac{2}{N_{ob}}} + 1 \approx 1 \tag{7a}$$

$$\left|\Delta J_{tg}\right| < \Delta_{\text{stop}} \tag{7b}$$

$$\left|\frac{J_{tg}}{J_{fg}}\right| < 10^{-6}, \tag{7c}$$

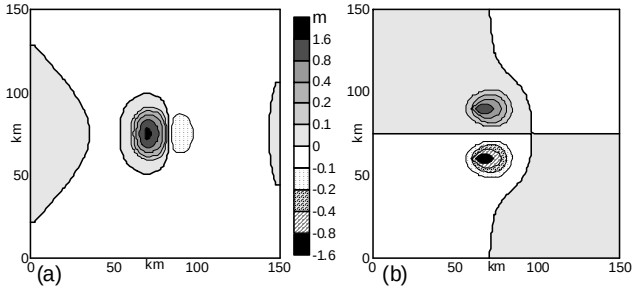

Fig. 2. Tsunami sources used to produce the tide gauge data (initial conditions): **(a)** pure dip-slip fault; **(b)** pure strike-slip fault.

where P_{95} is 95$^{\text{th}}$ percentile of the standard Gaussian distribution and Δ_{stop} is an arbitrary threshold, taken here as $10^{-3}N_{ob}\sigma_{ob}^2$. Equation (7a) tests if the noise level is significantly greater than the quadratic misfit (J_{tg}), assuming that the distribution error is white Gaussian noise and that N_{ob} is large enough to justify the substitution of a N_{ob}-degrees of freedom χ^2 distribution by a Gaussian distribution. Equation (7b) puts a bound on the variation of J_{tg} between consecutive iterations and stops the iteration in cases where the existence of model errors or of a too restrictive control vector does not allow for a convergence to the true solution. Equation (7c) takes into account round-off errors. A detailed discussion of the stopping criteria in optimization can be found, for example, in Fletcher (1987).

In the case of the inversion of synthetic data, one can compute the goodness of the solution as the relative average error, ε, or the L2-norm misfit, between the true field $\varsigma_i^{\text{true}}$ and the inverted ς_i^{in} surface displacement field, at the initial time:

$$\varepsilon = \left[\frac{\sum_i \left(\varsigma_i^{\text{true}} - \varsigma_i^{\text{in}}\right)^2}{\sum_i (\varsigma_i^{\text{true}})^2} \right]^{1/2}, \tag{8}$$

where the sum spans over all the spatial domain. Other measures of the misfit, also used in this paper, which do not require the knowledge of the true initial state, are the relative change of the cost function (J_{tg}/J_{fg}) and ratio between the cost function and the noise level $J_{tg}/(N_{ob}\sigma_{ob}^2)$.

The inversion method to be applied consists in the 4 following steps: (1) Objective spatial delimitation of the tsunami source by the adjoint method (Sect. 4). This consists in the establishment of a control vector that is a restriction of ς_0 in the target area, and is the adjoint equivalent of the backward ray-tracing technique (Miyake, 1934; Abe, 1973); (2) Adjoint optimization of the initial state in the target area (Sect. 5), starting from a vanishing first guess ($V_{\text{inv}} = 0$); (3) Non-linear least-square adjustment of the fault parameters by minimization of the averaged-square misfit between the inverted initial field and the Okada (1992) model, from an "educated guess" (Sect. 7); (4) Final optimization of the initial state by the adjoint method in the fault parameter space, by minimization of the misfit of the tide gauge data, with a first guess issued from the previous step (Sect. 7).

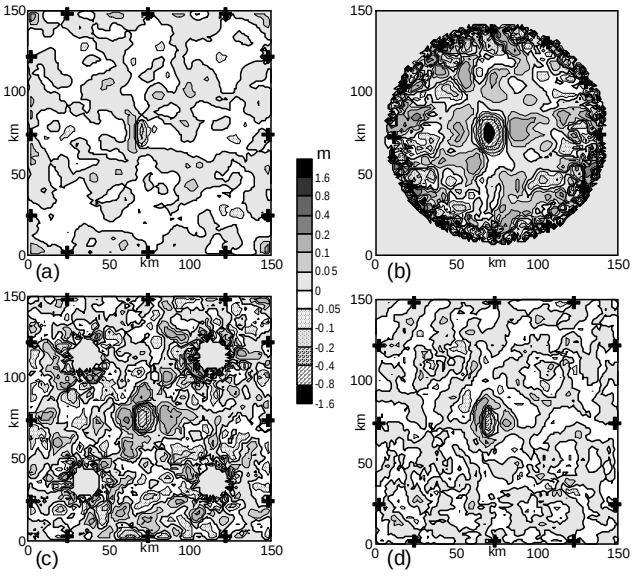

Fig. 3. Inversion error for the domains shown in Fig. 1, in unconstrained inversions with no observation error: **(a)** open flat domain; **(b)** closed lake; **(c)** open domain with islands; **(d)** open domain with submarine mountains. The location of tide-gauge stations is represented by crosses. Note the geometric scale.

3 Experiment set-up

In all experiments, the computational domain consists of a 150 km×150 km square, with four different bathymetry fields and coastline configurations (Fig. 1a–d), expressed as: (a) flat 200 m bathymetry, in an open domain (Fig. 1a); (b) closed lake, with depth increasing linearly from its centre at 200 m (Fig. 1b); (c) set of 4 islands in an open domain (Fig. 1c); (b) set of 4 submarine mountains in an open domain (Fig. 1d).

In all experiments the depth varies smoothly in the domain, with maximum depth at 200 m, and 12 tide gauges are evenly distributed at the boundaries (crosses in Fig. 1). These idealized domains allow for the assessment of the effects of the side boundaries, steep bathymetry and simple dispersion effects in the inversion of tsunami data. The model grid is always set at 2 km×2 km, and a 10 s time step is used, satisfying the CFL stability condition. A perturbation in the centre of the domain will take 15–25 min to reach the boundaries.

Two exact solutions generated by Okada (1992) formulas were tested for inversion (Table 2 and Figs. 2a, b) centred in the middle of the domain: pure dip-slip fault (Ok1), strike-slip fault (Ok2). As shown in Fig. 2, the crest and trough of source Ok2 are more distinctly separated in space than those of source Ok1.

In most experiments, observations taken at the tide gauges were modified by the addition of a white noise Gaussian perturbation with a standard deviation equal to 10% of the standard variation (σ_{syn}) of the synthetic waveforms. The inversions were performed with a 100 min assimilation period and with observations taken every 60 s ($N_{ob} = 1200$). In

Table 2. Fault parameters of the seismic sources

	$\delta(^\circ)$	d(km)	U_{sl}(m)	U_{st}(m)	x_0(km)	x_0(km)	$\alpha(^\circ)$	L(km)	W(km)
Ok1	30	8.750	5	0	75	75	0	15	15
Ok2	30	8.750	0	5	75	75	0	15	15
Okfg	0	5.000	0	0	75	75	0	30	30
Ok1inv	30.22	8.754	4.963	0.031	74.92	75.03	0.0048	15.12	14.93
Ok2inv	30.30	8.801	−0.018	5.041	74.85	74.97	0.1286	14.97	14.91

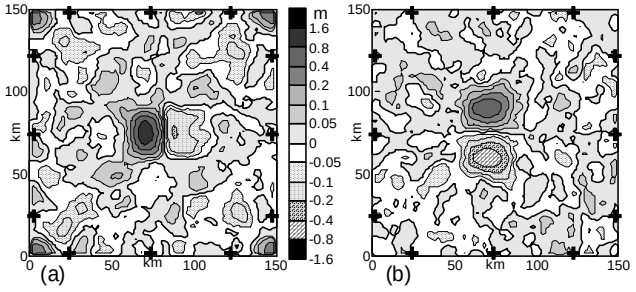

Fig. 4. Initial fields obtained by unconstrained adjoint inversion for the case of flat bathymetry and for **(a)** Exp. 5, pure dip-slip fault and **(b)** Exp. 10, strike-slip fault.

sensitivity experiments some parameters of the setup will be changed, to assess their impact on the solution error.

4 Unconstrained inversion experiments

As previously mentioned, the unconstrained inversion of tsunami data is an ill-posed problem. Even in the case of perfect-model simulations and error-free data ($\sigma_{ob} = 0$), it is not possible to obtain the initial fields. Figure 3 shows the spatial distribution of inversion errors, for the unconstrained inversion by the adjoint model, in the 4 bathymetric setups for the Ok1 source. The location of the tide gauge stations is also shown in the corresponding figures. In all cases, the maximum error is comparable with the maximum water displacement of the true source. Errors are large near the centre of the source, but also in other areas of the domain, where its distribution is closely related with bathymetric and boundary effects. In the case of open flat bathymetry, the error concentrates near the boundaries in between the observation points, where any initial perturbation will move out of the domain. This is a well-known problem with open domains (e.g. Tinti et al., 1996). In case of sloping bathymetry, waves are dispersed and loose coherency leading to a degradation of the inversion process. In these cases, spurious dipole-like sources appear in shallower locations, where the propagation speed is much lower leading to a reduction of the information content of wave forms for a fixed assimilation period. That effect is very strong near the coast in both closed (Fig. 3b) and open (Fig. 3c) domains. In the case of Fig. 3c, the dispersion effect of islands is very strong for tide gauges which are behind the islands. The dispersion effect of sea mountains is less pronounced but is highly relevant, as shown in the inversion of real tsunamis (e.g. Gjevik et al., 1997; PM01). Table 3 presents an overview of the inversion model performance in all unconstrained inversion experiments.

As shown in Table 3, in the absence of assumed observation error, the minimization stopped by a round-off criterion. On the other hand, the addition of observation noise leads to an earlier stop of the iteration, although at a larger error value. Bathymetry (b) leads to the worst solution, followed by (c), (d) and (a). Figure 4 presents the final inverted initial sea state for sources Ok1 (Fig. 4a) and Ok2 (Fig. 4b), in the case of an open flat bathymetry, to be compared with Fig. 2a, b.

5 Source delimitation by the adjoint method

As shown by PM01 and Piatanesi et al. (2001), area delimitation is a known solution to the ill-conditioning of the inversion problem discussed in Sect. 4. This can be done by classic backward ray-tracing, with arrival times visually estimated from the observed waveforms (e.g. Gjevik et al., 1997). However, a single integration of the adjoint model (5a–c), with a forcing consisting of a unitary impulse at each tide gauge point at the corresponding estimated tsunami arrival time N_{arr}, may directly provide the bound of the forbidden source area. The earlier is the estimated tsunami arrival time (small N_{arr}) the broader is the allowed domain for the source. Therefore, N_{arr} must be small enough to avoid the possibility of empty sources, while being large enough to constitute an efficient spatial constraint. We propose an objective criterion that works even in the presence of a reasonable observation error. Let N_a be a time step such that

$$\left|\varsigma_j\right| \leq \varsigma_{th},\ \forall j \leq N_a, \tag{9a}$$

where ς_{th} is a threshold, sufficiently distinct from the observation error, which can be taken as a criterion for the arrival of the leading wave. A compromise is obtained choosing

$$\varsigma_{th} = \max\left\{2\sigma_{ob},\ 0.1\sigma_{\text{syn}}\right\}. \tag{9b}$$

N_a is a first estimate of the arrival time. For noisy tide-gauge series, there is an initial time interval in which the sea-surface displacement associated with the leading wave is obscured by the observation noise. Because of that, N_a is an upper

Table 3. Unconstrained inversions

Exp	Source	Bathymetry	$\sigma_{ob}/\sigma_{\text{syn}}$ (%)	# iter	ε (%)	J_{tg}/J_{fg}	$J_{tg}/(N_{ob}\sigma_{ob}^2)$
1	Ok1	a	0	192	21.9	7.99×10^{-6}	∞
2	Ok1	b	0	198	87.3	8.59×10^{-5}	∞
3	Ok1	c	0	193	53.0	5.52×10^{-5}	∞
4	Ok1	d	0	194	24.3	4.24×10^{-5}	∞
5	Ok1	a	10	11	47.2	6.57×10^{-3}	0.67
6	Ok1	b	10	30	88.1	7.78×10^{-3}	0.79
7	Ok1	c	10	17	65.2	7.33×10^{-3}	0.76
8	Ok1	d	10	10	43.8	7.00×10^{-3}	0.71
9	Ok2	a	0	191	27.5	1.02×10^{-6}	∞
10	Ok2	a	10	8	40.0	7.77×10^{-3}	0.79

Table 4. Area-constrained inversions

Experiment	Source	Bathymetry	$\sigma_{ob}/\sigma_{\text{syn}}$ (%)	# iter	ε (%)	J_{tg}/J_{fg}	$J_{tg}/(N_{ob}\sigma_{ob}^2)$
5a	Ok1	a	10	7	9.6	7.96×10^{-3}	0.81
5aOk	Ok1	a	10	7+51	1.4	9.23×10^{-3}	0.94
6a	Ok1	b	10	21	21.4	11.9×10^{-3}	1.22
7a	Ok1	c	10	23	16.2	9.33×10^{-3}	0.96
8a	Ok1	d	10	12	14.3	7.91×10^{-3}	0.80
10a	Ok2	a	10	12	17.7	17.3×10^{-3}	1.76
10aOk	Ok2	a	10	12+130	1.1	9.53×10^{-3}	0.97

bound to the true arrival time, and we can obtain an improved estimation of the arrival time as:

$$N_{arr} = N_a - N_{\text{lead}}, \tag{9b}$$

where, N_{lead} is the time taken from the first estimate of the arrival (N_a) to the maximum displacement in the leading wave. Criterion (9a–c) was tested and tuned with synthetic data. Figure 6b shows the result obtained, for tide gauge X in Fig. 1a, and Experiment 5.

The adjoint model is then integrated from N_{arr} to the origin of time, giving the gradient $G = \partial\varsigma_{arr}/\partial\varsigma_0$. For point sources that are too far away from the tide gauge, $G \sim \varepsilon_{th}$ (round-off error, taken as 10^{-6}), indicating that the sea-level perturbations in those points at the initial time cannot propagate to the gauge in the available time interval (N_{arr}). The backward wave front at the initial time is then located at the boundary of the region, where $|G| < \varepsilon_{th}$. Each tide gauge will then lead to a decomposition of the domain in two regions: the forbidden region (too close to the gauge for the computed arrival time) and the allowed region. One will define, for each tide gauge k, a field:

$$A_k(x,\ y) = \min\left\{\frac{\varepsilon_{th}}{|G(x,\ y)|},\ 1\right\} \in [0,\ 1]. \tag{10}$$

The sum of $A_k(x,\ y)(k = 1, ...12)$, over all 12 tide gauge, corresponds to the number of stations where tide-gauge arrivals are compatible with a point source at $(x,\ y)$. That sum is shown in Fig. 5, corresponding to Experiments 5–8. The areas where that field takes the value 12 (equal to the num-

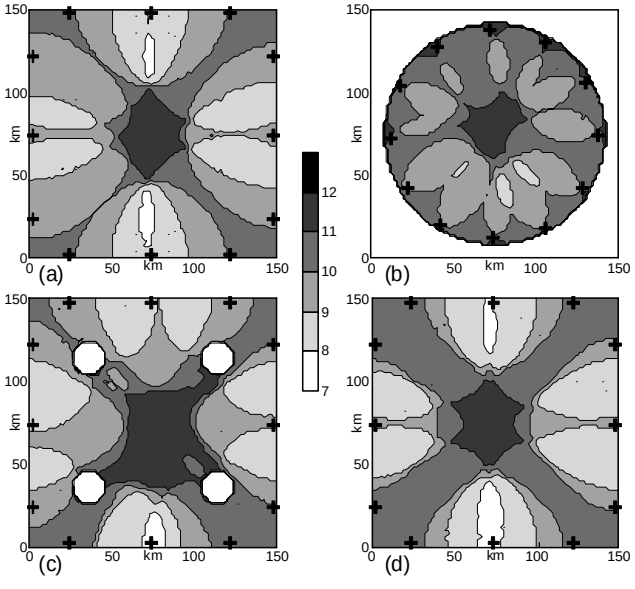

Fig. 5. Area delimitation by the adjoint method. Shading represents the number of stations compatible with the source at that location for: **(a)** open flat domain; **(b)** closed lake; (c) open domain with islands; (d) open domain with submarine mountains.

Table 5. Sensitivity experiments

Experiment	Test	# iter	ε (%)	J_{tg}/J_{fg}	$J_{tg}/(N_{ob}\sigma_{ob}^2)$
5a	Control	7	9.6	7.96×10^{-3}	0.81
5b	Assimilation period = 40 min	12	14.7	8.71×10^{-3}	0.88
5c	Assimilation period = 200 min	6	8.4	9.21×10^{-3}	0.93
5d	Sampling 120 s	8	35.4	7.54×10^{-3}	0.77
5e	Sampling 10 s	7	7.3	11.4×10^{-3}	1.16
5f	4 tide gauges	10	21.9	7.75×10^{-3}	0.79
5g	24 tide gauges	6	8.5	9.60×10^{-3}	0.97
5h	Bathymetric error = 10 m	8	16.8	9.09×10^{-3}	0.92
5i	Bathymetric error = 20 m	6	21.8	20.9×10^{-3}	2.13
5j	Observation error, $\sigma_{ob} = 20\%$	4	15.1	29.8×10^{-3}	0.78
5k	Observation error, $\sigma_{ob} = 50\%$	3	29.1	139×10^{-3}	0.69

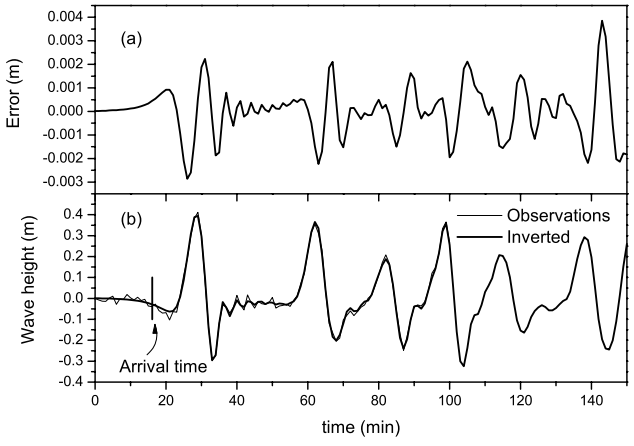

Fig. 6. Results from Exp. 5a at the X gauge (Fig 1a): **(a)** Inversion error – difference between the inverted solution and the truth; **(b)** Comparison between observations and inverted solution. In (b) the arrival time computed with Eq. (9) is also shown.

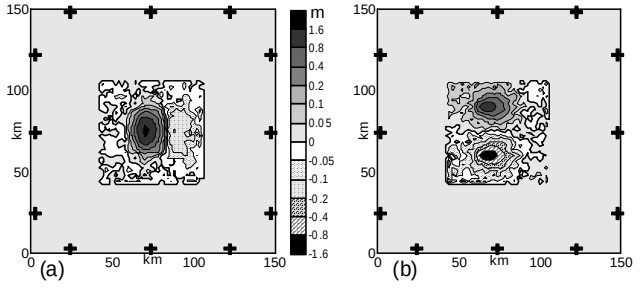

Fig. 7. Initial fields obtained by the adjoint inversion of data from: **(a)** Exp. 5a; **(b)** Exp. 10a.

ber of gauges) is where a source is compatible with all arrival times, and it does indeed contain the main true source area, supporting the described methodology. The geometry of the area delimitation results (Fig. 5) shows, again, the inversion problems in the four bathymetric setups, namely the occurrence of wake effects behind the islands and the large uncertainty in shallow areas.

The area obtained by delimitation was then simplified to a centred 60 km×60 km square, shown in Fig. 1a. The delimited area was taken as a control vector for the second step of optimization, leading after a number of iterations to new initial fields. Table 4 lists the main results of the new experiments. In all cases, one finds a decrease of the relative error. In the case of source Ok2 (Exp. 10a), the stopping criterion was given by Eq. (7b), indicating that the source is not well represented in the limited domain.

Figure 6 shows the wave forms obtained at gauge X for Experiment 5a. Figure 6a shows the inversion error (difference between computed and true wave forms, where the true wave forms have no observation error) and the comparison between observations (truth+error) and computed wave forms. It can be concluded that the method was able to get rid of the (10%) observation error in the inversion process, leading, in this idealized case, to negligible error (∼1%).

Figure 7a shows the initial water displacement field for the Exp. 5a, while Fig. 7b shows the corresponding field for Exp. 10a. Those figures are in good agreement with the true solution (Fig. 2a, b) but it is clear that they still exhibit significant noise. The evolution of the cost function (J_{tg}/J_{fg}) and of the relative error (Eq. 8) are shown in Fig. 8. As shown in Table 4, the optimal solution in the experiments with a 10% noise level was obtained in a small number of iterations (7–23) with a reduction of the inversion error by a factor of 2–4. The larger relative reductions in inversion error were obtained in the case of the closed lake, where the area elimination prohibited the spurious sources in coastal waters.

6 Inversion sensitivity

To test the sensitivity of the inversion model to the different parameters, a number of experiments were designed, where those parameters are varied. To simplify the analysis, Exp. 5a was taken as the control experiments and parameters are

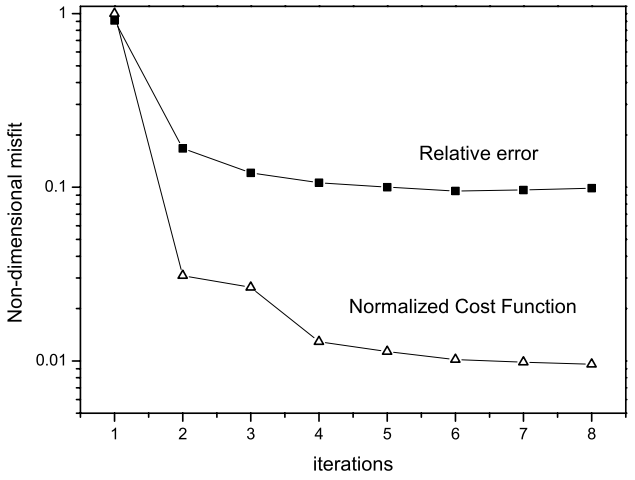

Fig. 8. Evolution of the relative error (ε) and of the normalized cost function (J_{tg}/J_{fg}) in Exp. 5a.

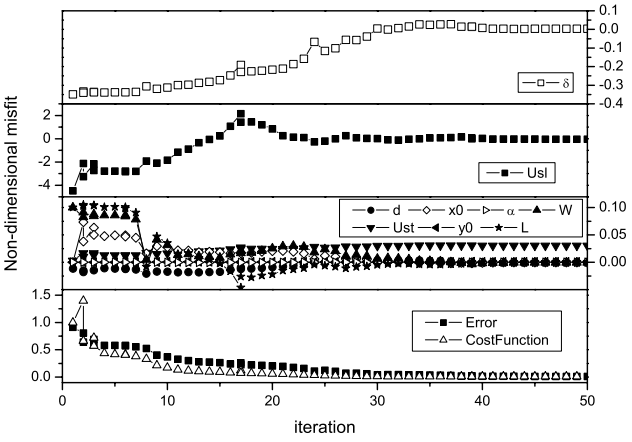

Fig. 9. Evolution of the misfit of the fault parameters, of the normalized cost function (square misfit between Okada source and distributed source, normalized its first-guess value) and of the relative error, in steps 3 and 4 of the adjoint inversion (fault parameter adjustment) in Exp. 5aOk.

varied, one by one, in each experiment. Table 5 describes that set of experiments. Exp. 5b and 5c test the effect of the extension of the assimilation period; as expected, the error varies monotonically with that period. Exp. 5d and 5e test the effect of sampling interval; note that this is the tide gauge sampling and not the model time step that is fixed at 10 s. Exp. 5f and 5g test the effect of the number of observation points, which are in all cases regularly distributed around the domain. In all cases, the error decreases monotonically with the number of available data. Exp. 5h and 5i test the effect of including bathymetric errors. In those two experiments a white noise Gaussian was added to the depth (200 m) at each grid point, with a standard deviation of 10 or 20 m. As expected, bathymetric errors strongly degraded the model performance, and criterion given by Eq. (7b) was applied to turn off the minimization. Finally, Exp. 5j and 5k test the effect of large observation errors, which, while significantly degrading the results, can still be sensibly inverted.

There are many other potential error sources in this problem. As shown in PM01 and Piatanesi et al. (2001) the azimuthal coverage is an important constrain in the solution. In practice, clock errors and different model errors have to be taken into account.

7 Fault parameters inversion

One can now proceed to the final stages of the optimization (steps 3 and 4). Using the solutions obtained in Exp. 5a and 10a, one can now iterate to obtain the best fit with the Okada model, solving a non-linear least-square problem using a gradient-descent method. Figure 9 shows the evolution of the normalized fault parameters ((inverted-exact)/scale, cf. Table 1 and 2) during the optimization process. In Fig. 9, the multiple values for the same iteration correspond to intermediate simulations of the minimization algorithm. The first guess in the optimization process is also shown in Table 2 (Okfg) and it contains little a priori information on the fault solution. A number of alternative first-guess's were tested with similar final results. However, one may need to test several first-guess's and compare their final solutions in order to avoid the convergence to local (not absolute) minima of the misfit in the parameter space. In the present case, all parameters converged to values close to the exact solution in about 50 iterations, reducing the relative error from 9.62 to 1.42%. This ends step 3.

Starting from the first guess obtained in step 3, one will now apply, again, the adjoint variational optimization of the initial field, by minimization of the misfit of the tide gauge data (J_{tg}), but restricting the control vector to the 9 Okada-scaled parameters. Steps 3 and 4 could be merged, but that may imply difficulties in reaching the absolute minimum of the misfit, due to the strong constrains imposed by the Okada model. The convergence of this last step occurs in just 2 iterations, also shown in Fig. 9. Final parameters are presented in Table 2 (Ok1inv, Ok2inv), the inversion data is given in Table 4 (Exp. 5aOk and 10aOk) and the corresponding water displacement fields are shown in Fig. 10a, b, to be compared with Fig. 2a, b. It is clear that the constrained inversion in the fault parameter space had a major impact in the quality of the solution, with a reduction of the relative error by an order of magnitude (cf. Tables 3 and 4).

The errors in the scaled parameters have a Gaussian distribution, since they are approximate linear transformations of the Gaussian observational error. The expected value of the inversion errors is zero, since the inversion model is taken as perfect and the observational errors are unbiased. Taking into account the covariance structure of the observation errors, the error-covariance matrix of the scaled Okada parameters, C, or resolution matrix, can be computed through the Hessian matrix of the cost-function, given by Eq. (3) (PM01):

$$C = \mathrm{cov}\,(\varepsilon_{\mathrm{inv}},\ \varepsilon_{\mathrm{inv}}) = 2\sigma_{ob}^2 H^{-1}, \qquad (11)$$

Table 6. Components of the nine eigenvectors of C over the 9 scaled Okada parameters, for the dip-slip fault inversion

k	$\hat{\delta}$	$\hat{d}$	$\hat{U}_{sl}$	$\hat{U}_{st}$	$\hat{x}_0$	$\hat{y}_0$	$\hat{\alpha}$	$\hat{L}$	$\hat{W}$	$\sigma_{ok,k}$	$\varepsilon_{ok,k}$
1	0.038	0.008	**0.999**	0.018	−0.004	4.67×10^{-6}	0.005	−0.009	−0.011	0.045	−0.036
2	−0.001	−0.0003	−0.018	**0.999**	0.0002	−0.005	−0.003	−0.0005	0.0005	0.019	0.031
3	0.020	0.0007	−0.006	0.003	0.001	0.026	**0.999**	0.0013	−0.0029	0.0053	0.00035
4	**0.990**	0.0438	−0.038	0.0009	−0.079	0.0005	−0.021	0.038	−0.085	0.0037	0.0054
5	0.093	0.167	−0.002	−0.0006	0.167	−0.011	0.0015	**–0.634**	**0.729**	0.00057	0.0005
6	−0.029	**0.847**	0.0016	0.0004	0.120	0.0023	-2.7×10^{-6}	**0.477**	0.198	0.00034	0.0001
7	0.060	**–0.496**	0.015	3.4×10^{-5}	0.104	−0.025	0.001	**0.606**	**0.608**	0.00021	−0.0002
8	0.0012	−0.012	0.0004	0.005	0.0005	**0.999**	−0.026	0.0073	0.023	0.00016	0.00041
9	0.062	−0.077	0.0004	-4.1×10^{-5}	**0.969**	0.0048	−0.0005	−0.012	0.222	0.00010	−0.00015

where H^{-1} is the inverse of the Hessian matrix of the cost function, numerically computed by differentiation of its gradient, already obtained by the adjoint method. The resolution matrix can be analysed to provide information on the relative error of the inverted parameters. The parameter errors are correlated, implying that C is non-diagonal, and one must solve the eigenvalue problem to obtain the directions in the error-space in which the error is worst and best resolved. On the other hand, each eigenvalue, λ_k, of C is the variance of the error component in the corresponding unitary eigenvector. Table 6 shows the components of the normalized nine eigenvectors of C, for decreasing eigenvalue, over the nine scaled Okada parameters (where scaling is represented by the symbol $\hat{}$), for experiment 5aOk. Leading components, contributing more than 5% to the eigenvector norm, appear in bold. In that table, $\sigma_{ok,k} = \sqrt{\lambda_k}$ represents the standard deviation of the k^{th}-component error in the eigenvector basis of the scaled Okada parameters. In the same table, the variable $\varepsilon_{ok,k}$ represents the corresponding verifying error (exact-inverted). As expected, both $\sigma_{ok,k}$ and $\varepsilon_{ok,k}$ decrease with the order of the eigenvector and are of comparable magnitude. The best resolved parameters, which project strongly in the higher order eigenvectors, are the fault position (x_0, y_o), while the dislocation lengths (U_{sl}, U_{st}) are poorly resolved, being mainly projected in the leading eigenvectors. Table 6 also shows that, while most eigenvectors project strongly on a single Okada parameter, the parameters d, L and W contribute together to the three eigenvectors (5, 6, 7). This may have some geophysical importance, as it implies that the inversion of each of those parameters, from tide-gauge data, can not be done independently. From a hydrodynamical point of view the interconnection between d, L and W, comes from the fact that a deeper but more extended fault may produce an initial water displacement similar to a shallower and narrower fault.

Figures 11a, b show the distribution of $J' = \ln(J_{tg}/(N_{ob}\sigma_{ob}^2))$, in the eigenvector space. The size of the axis of the ellipses $J' = 0$ in Fig. 11a, b are, as expected, of the order of the corresponding $\sigma_{ok,k}$ (Table 6). Similar results (not shown) were obtained for the strike-slip fault source (Exp. 10aOk).

8 Discussion and conclusions

The adjoint method offers a general approach to the problem of data inversion in geophysics. It allows for either linear or non-linear forward propagation models, which can allow for non-linear advection, dispersion and run-up effects, important in shallow areas, although at the cost of writing the corresponding adjoint codes. The adjoint method may explicitly include physical constrains on the solution, which may be given as a non-linear combination of a set of parameters, and it may deal with observation, model and bathymetric errors. This paper has applied the adjoint inversion methodology to the tsunami waveform inversion problem, extending the study by Pires and Miranda (2001) with a systematic sensitivity analysis.

The adjoint inversion method is highly flexible. It can be applied to the unconstrained inversion of distributed sources, where every grid point in the domain is considered a potential point source. In that case it is similar to Satake (1987) Green's functions method, although more general, because the linearity of the propagation model is not required. It can also be applied for area-constrained sources. The definition of the allowed source area may be obtained by the adjoint method itself, through a procedure that is equivalent to backward ray-tracing and that, as shown in this paper, does not require a subjective interpretation of the tide gauge signals and can deal with reasonable amounts of observational error. Finally, the adjoint method can invert sources that explicitly satisfy the Okada (1992) fault model or other well-behaved non-linear physical models.

The inversion methodology developed in this paper consists in 4 steps: (i) area delimitation by adjoint backward ray-tracing; (ii) adjoint inversion of a limited-area distributed source; (iii) selection of the best-fit Okada source; (iv) further adjoint inversion of the Okada source from the first guess issued from (iii). In the analysis of synthetic data, this 4-step methodology was found to converge to a solution very close to the true solution, with relative errors of the order of 1%, in cases where a 10% noise level was added to the "observations".

Real seismic tsunami sources do not follow the idealized

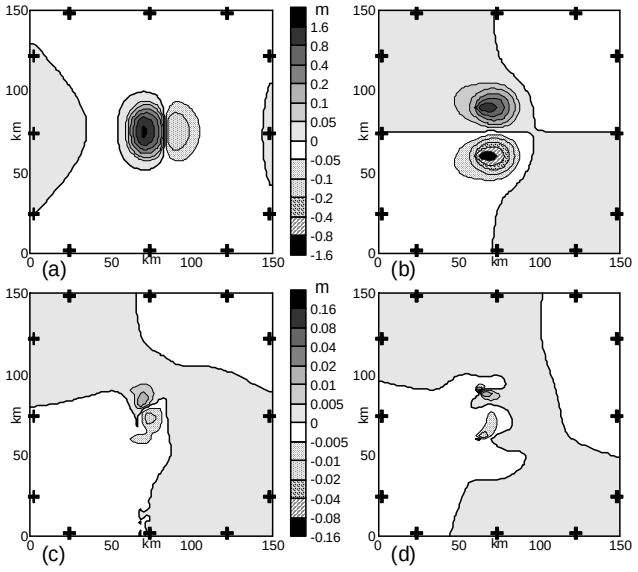

Fig. 10. Final inverted initial fields, by adjoint optimization of the fault parameters, and error distribution, in the experiments with open flat domain and 10% observation error, for the two sources: **(a)** pure dip-slip fault solution; **(b)** strike-slip fault solution; **(c)** pure dip-slip fault error; **(d)** strike-slip fault error. Note the difference in scale between the solution and the errors.

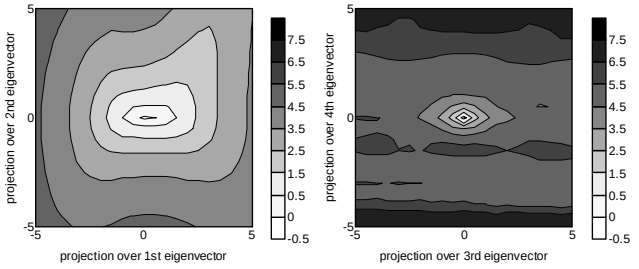

Fig. 11. Distribution of $\ln(J_{tg}/(N_{ob}\sigma_{ob}^2))$ in the space span by the four more relevant eigenvectors of the covariance error matrix of the scaled fault parameters.

fault model proposed by Okada (1992). Real tsunamis have heterogeneity and if data were available one could argue that it could be better to stop the inversion process in step (ii). The problem, though, is the fact that data is generally largely insufficient to support the inversion of the large number of independent parameters implied by the distributed source model and solutions will be, most likely, polluted by data and model errors. In that context it seems much more interesting to have a more robust estimate of much fewer parameters, such as a subset of the fault parameters, which can be independently checked by solid earth geophysical analysis. That robust estimate can be provided by the adjoint model. The inclusion of geophysical data into the cost-function is also manageable by the adjoint method.

As applies to other waveform inversion methods, the adjoint inversion is highly dependent on the signal-to-noise ratio. In this study, that ratio was imposed, but one should expect that it may vary substantially from case to case, depending not only on the instrumental setup but also on the location and nature of the source. If the signal amplitude at the tide-gauges is very small, as in far-field tsunamis or when the source transfers little potential energy to the water column, the method will lead to less reliable results.

The methodology proposed by Pires and Miranda (2001), and further developed in this paper, can be extended to the inversion of other source models, not necessarily of seismic origin. The method can also provide information on the inversion error associated with different parameters and parameter combinations. The error covariance matrix of the inverted parameters (resolution matrix) is obtained as a by-product of the adjoint method and its eigenvector decomposition gives the main directions of error projection, allowing for the identification of the more uncertain parameters in the inversion.

Acknowledgements. Suggestions from two anonymous referees contributed to improve this paper. This work was carried out at the Centro de Geofisica da Universidade de Lisboa (CGUL) with funds from the Portuguese Science Foundation (FCT) under Grant PRAXIS/C/CTE/11050/1998 (IMETFOR), which is co-financed by the European Union under program FEDER.

References

Abe, K.: Tsunami and mechanisms of great earthquakes, Phys. Earth Planet. Inter., 7, 143–153, 1973.

Baptista, M. A., Miranda, P. M. A., Miranda, J. M., and Mendes-Victor, L.: Constraints on the source of the 1755 Lisbon tsunami inferred from numerical modeling of historical data, J. Geodyn., 25, 159–174, 1998.

Bennett, A. F.: Inverse Methods in Physical Oceanography, Cambridge Univ. Press, New York, 346, 1992.

Fletcher, R.: Practical methods of optimization, John Wiley & Sons, 2nd ed., 436, 1987.

Ghil, M. and Malanotte-Rizzoli, P.: Data assimilation in meteorology and oceanography, Adv. Geophys., 33, 141–266, 1991.

Gilbert, J. C. and LeMaréchal, C.: Some numerical experiments with variable-storage quasi-Newton algorithms, Math. Programming, 45, 407–435, 1989.

Gjevik, B., Pedersen, G., Dybesland, E., Harbitz, C. B., Miranda, P. M. A., Baptista, M. A., Mendes-Victor, L., Heinrich, P., Roche, R., and Guesmia, M.: Modeling tsunamis from earthquake sources near Gorringe Bank southwest of Portugal, J. Geophys. Res., 102, 27 931–27 949, 1997.

Johnson, J. M., Satake, K., Holdahl, S. R., and Sauber, J.: The 1964 Prince William Sound earthquake: Joint inversion of tsunami and geodetic data, J. Geophys. Res., 101, 523–532, 1996.

Johnson, J. M.: Heterogeneous coupling along Alaska-Aleutians as inferred from tsunami, seismic, and geodetic inversions, in Tsunamigenic Earthquakes and their Consequences, edited by Dmowska, R. and Saltzman, B., Adv. Geophys., 1–116, 39, 1999.

Koike, N. and Imamura, F.: Application of the inversion method to a real-time far-field tsunami forecast system, ITS 2001 Proceedings, Session 7, 2001.

Miyabe, N.: An Investigation of the Sanriku Tsunami based on mareogram data, Bull. of the Earthquake Res. Inst., Tokyo University, Suppl., 1, 112–126, 1934.

Okada, Y.: Internal deformation due to shear and tensile faults in a half-space, Bull. Seismol. Soc. Am., 82, 1018–1040, 1992.

Piatanesi, A., Tinti, S., and Pagnoni, G.: Tsunami waveform inversion by numerical finite-elements Green's functions, Natural Hazards and Earth System Science, 1, 187–194, 2001.

Pires, C. and Miranda, P. M. A.: Tsunami waveform inversion by adjoint methods, J. Geophys. Res., 106, C9, 19 773–19 796, 2001.

Pires, C., Vautard, R., and Talagrand, O.: On extending the limits of variational assimilation in nonlinear chaotic systems, Tellus, 48A, 96–121, 1996.

Satake, K.: Inversion of tsunami waveforms for the estimation of a fault heterogeneity: Method and numerical experiments, J. Phys. Earth, 35, 241–254, 1987.

Satake, K.: Inversion of tsunami waveforms for the estimation of heterogeneous fault motion of large submarine earthquakes: The 1968 Tokachi-oki and 1983 Japan Sea earthquakes, J. Geophys. Res., 94, 5627–5636, 1989.

Talagrand, O., and Courtier, P.: Variational assimilation of meteorological observations with the adjoint vorticity equation, I, Theory, Q. J. R. Meteorol. Soc., 113, 1311–1328, 1987.

Tinti, S., Piatanesi, A., and Bortolucci, E.: The finite-element wave propagator approach and the tsunami inversion problem, Phys. Chem. Earth, 21, 27–32, 1996.

Wunsch, C.: The Ocean Circulation Inverse Problem, Cambridge Univ. Press, New York, 456pp., 1996.